

Probing the elastic properties of individual nanostructures by combining *in situ* atomic force microscopy and micro-x-ray diffraction

T. Scheler,¹ M. Rodrigues,¹ T. W. Cornelius,¹ C. Mocuta,¹ A. Malachias,¹ R. Magalhães-Paniago,¹ F. Comin,¹ J. Chevrier,^{1,2} and T. H. Metzger^{1,a)}

¹European Synchrotron Radiation Facility (ESRF), B.P. 220, 38043 Grenoble, Cedex, France

²Institut Néel, CNRS-UJF, B.P. 166, 38042 Grenoble, Cedex 9, France

(Received 6 November 2008; accepted 16 December 2008; published online 16 January 2009)

Atomic force microscopy (AFM) and micro-x-ray diffraction are combined to investigate nanostructures during *in situ* indentation. This technique allows the determination of elastic properties of individual nanoscale objects, particularly here SiGe/Si(001) self-assembled islands. Using this novel technique it was possible to select a specific island, align it in the microfocused beam, and apply a pressure onto it, using the AFM tip. Simultaneously, the x-ray diffuse scattering map from the island and the surrounding substrate was recorded in order to probe the lattice parameter change during indentation. An elastic reduction of the island lattice parameter of up to 0.6% was achieved. © 2009 American Institute of Physics. [DOI: 10.1063/1.3067988]

Semiconductor nanostructures, both self-assembled and artificially formed by lithography, play a key role in the development of devices based on nanotechnology. Their electronic and structural properties have been investigated extensively in the past.¹ While the mechanical behavior of bulk materials is well-understood, a change is expected when the size of these objects is reduced to below a certain limit.² The combination of scanning probe microscopy and synchrotron radiation is extremely useful in the study of nanostructures.³ In this context, x-ray diffraction (XRD) has been developed as a standard tool to investigate shape, composition, and strain of nanosized objects.⁴ Usually, near millimeter-sized beams are employed and thus yield statistically averaged information about the nanostructures. In order to study individual objects, it is necessary to focus the beam to an adequate size, typically in the (sub-)micron regime. For x-rays this can be achieved using, e.g., compound refractive Be lenses.⁵ However, with such a small x-ray beam, the simultaneous alignment, manipulation, and investigation of nanostructures present a particular experimental challenge. In recent years, several techniques for nanoindentation have been developed and by now these methods serve as important tools in the investigation of the mechanical properties in the nanometer range.⁶ Up to now it was impossible to investigate the *elastic* regime of deformation of small structures due to the lack of *in situ* information about the indentation process. Commercially available atomic force microscopes enable the manipulation of nanostructures but cannot be integrated into a setup at synchrotron based x-ray beamlines.

In the present study we used SiGe/Si(001) self-assembled islands, a well-understood model system,⁴ to explore the potential of a combined *in situ* atomic force microscopy (AFM) and micro-x-ray diffraction (μ -XRD) setup. For this purpose we used a novel AFM developed at the ESRF in Grenoble, France, and integrated it into the diffractometer setup at beamline ID01.⁷ Figure 1(a) shows a schematic overview of the setup. The energy of the synchrotron radiation is selected by a double-bounce channel-cut Si(111) monochromator yielding a nearly parallel x-ray wave front

with a band width of $\Delta E/E = 1.2 \times 10^{-4}$. The monochromatic x-ray beam of 9.90 keV is subsequently focused by a stack of 32 Beryllium lenses placed 750 mm in front of the sample. The AFM tip is aligned in the focused x-ray beam, with a spot size of $1.5 \times 2.8 \mu\text{m}^2$ (full width half maximum, vertical \times horizontal), as schematically displayed in Fig. 1(b). The x-ray scattering from a single island, placed underneath the tip, and thus being in the microfocused beam, is measured by a Princeton PI-SCX-1300 two dimensional (2D) charge coupled device (CCD) detector.

The AFM uses a quartz tuning fork (TF) excited by a piezoelement with a typical resonance frequency of 32 768 Hz. As a tip we use an electrochemically etched tungsten wire with a diameter of 100 μm , which was glued to the lower prong of the TF by conductive silver epoxy adhesive. The resonance frequency is lowered to approximately 29.8 kHz due to the additional mass of the tip. The oscillation amplitude is in the order of a 2–3 nm. In order to be used as both a scanning probe and an indentation device, the

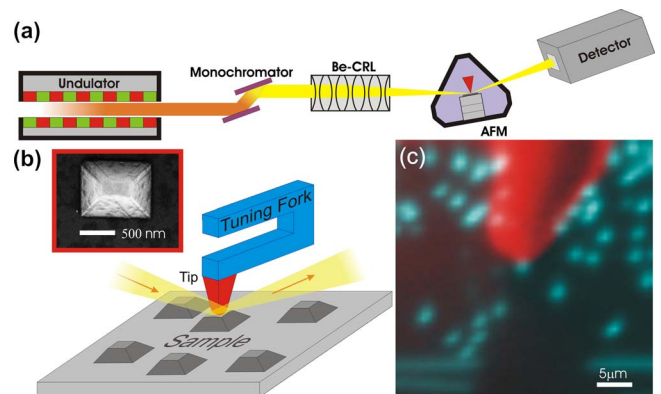


FIG. 1. (Color online) (a) Schematics of the *in situ* AFM and μ -XRD setup. The monochromatic x-ray beam is focused on the AFM tip and sample. The diffraction pattern is recorded by a 2D array detector. (b) Detail of the AFM placed in the focused x-ray beam. The AFM tip is shown in red. The inset shows a scanning electron micrograph of the island and its facets. (c) Superposition of two images of the sample: scanning XRD microscopy image of the sample surface (blue, sensitive to the SiGe islands) and beam induced photocurrent image showing the shape (red) and relative position of the AFM-tip on top of an isolated SiGe island.

^{a)}Electronic mail: metzger@esrf.fr.

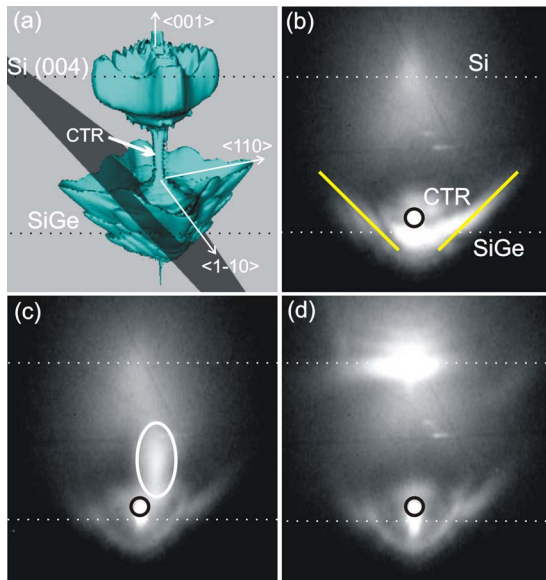


FIG. 2. (Color online) (a) 3D visualization of a simulated diffraction pattern (reciprocal space) from a SiGe island in the vicinity of the Si (004) Bragg peak (isointensity surface). The gray transparent plane depicts the interception of the reciprocal space by the detector plane for the images [(b)–(d)]. (b) 2D x-ray reciprocal space cuts for a noncompressed island. The flares highlighted in the figure (yellow lines) are the interception by the CCD plane of the $\langle 111 \rangle$ diffraction flares (panel a) originating from the island's $\{111\}$ side facets [(c) and (d)]. Same x-ray maps for medium pressure (c) and high pressure (d) where the island is fully compressed (see text for details). A complete series of images showing the variation of the scattering pattern is available online (multimedia file No. 1) (Ref. 12).

tip has to meet special requirements. Usually, the radius of curvature of an AFM tip has to be as small as possible enabling high resolution imaging. In our case, however, a sharp tip is inappropriate for indentation experiments and the tip has to be blunted to achieve an apex with a radius of curvature of a few micrometers. This deteriorates the imaging capabilities but they are still sufficient to identify single islands or to recognize predefined (interesting) areas with isolated objects, which were before selected on the sample [using *ex situ* imaging techniques, such as scanning electron microscopy (SEM) or AFM]. Laterally scanning the AFM position (sample and tip) in the x-ray microbeam and recording at each point a signal characteristic to the SiGe islands allows to obtain 2D maps of the sample surface and island position.^{8,9} At the same time, the photoelectrons produced by the x-ray beam illuminating the conductive tip can be used to image and align the tip with respect to the x-ray beam, with a precision comparable to the focus size. Figure 1(c) shows a scanning XRD microscopy^{8,9} image of the SiGe islands (blue) overlaid by the photocurrent signal (red) collected during scanning the tip-sample system through the much smaller focus. Combining the two techniques it is possible to align the x-ray beam precisely with respect to the AFM tip and, moreover, identify the chosen island in its vicinity. The tip can be positioned with high accuracy on top of an island using the AFM imaging capabilities

Figure 2(a) depicts the simulated diffraction map from a strained SiGe island and Si substrate close to the (004) Bragg peak expected to be measured in this experiment. Here we studied a single island with a shape of a truncated pyramid (rectangular basis) with $\langle 111 \rangle$ side facets, a base width of ~ 1000 nm, and height of ~ 400 nm [inset Fig. 1(b)].⁸ Its

nominal average Ge concentration is 14%, resulting in a SiGe lattice-parameter of 5.465 Å, as compared to 5.431 Å for silicon ($\Delta a/a=0.6\%$). The semitransparent plane in Fig. 2(a) shows the planar cuts in reciprocal space the 2D detector measures for a fixed incident angle. The center of the 2D detector was placed and kept fixed at an angle close to the maximum intensity of the SiGe(004) Bragg peak of the island.

In order to apply pressure on the island, the tip is brought into contact with the sample surface in tapping mode using the AFM feedback loop. At this point, the feedback is turned off and the piezovoltage of the positioning system is controlled manually. By changing the piezodisplacement Δz the force applied on the island is varied. Moreover, the TF prong is deflected due to the interaction with the sample. Since the TF is not mounted rigidly, it may move in its suspension and, thus, its deflection does not coincide with Δz . Consequently, the piezodisplacement cannot be employed for estimating force and pressure applied on the nanostructure under study but a more sophisticated model has to be developed to obtain these parameters. Figures 2(b)–2(d) shows the corresponding measured 2D reciprocal space maps (RSMs) before (b) and while (c) and (d) applying a pressure onto the island. The crystal truncation rod (CTR) from the Si substrate surface is marked by black circles. Note that its position does not change while pushing, indicating that no sample tilting is induced when the islands are compressed. Besides the strong peak, where the detector plane is cutting the diffraction signal characteristic to the SiGe island (lower dashed line), two flares of diffuse intensity pointing in $\langle 111 \rangle$ directions are observed, being the CTRs from the islands side facets [form factor scattering, yellow solid lines in Fig. 2(b)]. At the position of the Si substrate Bragg peak (upper dashed line) only a weak diffuse intensity is found, since the detector cuts the reciprocal space quite far away from the Si(004) Bragg peak [Fig. 2(a)]. While increasing the pressure in small steps, 2D-RSMs are recorded sequentially at every step (i.e., resulting in typically 30–40 data points), accessing simultaneously the applied tip pressure. With rising pressure on the individual SiGe island, the RSMs change dramatically. The SiGe signal [white circle in Fig. 2(c)] moves from its original position towards the Si peak, indicating a compression of the lattice parameter in the island.

For the highest pressure the SiGe island intensity maximum is superimposed onto the Si substrate peak, indicating an averaged lattice compression in the island of up to 0.6% (as expected for the Ge concentration of 14% in the islands) [Fig. 2(d)]. Thus, the lattice-parameter change in the island can be followed *in situ* as a function of the applied pressure which is derived applying the Hertzian contact model.¹⁰ The remaining diffuse scattering at the original SiGe island position stems from neighboring islands which are still illuminated by the weak extended tails of the focused x-ray beam, but are not affected by the AFM tip. We would like to emphasize that the original shape of the RSM is obtained again after the tip has been retracted in steps, proving that the island mechanical response was completely elastic. The measurement was repeated three times and was reproducible. Note that the effects observed in Figs. 2(b)–2(d) do not originate from the AFM tip or its z -movement in the x-ray beam; a similar experiment performed on a region containing the bare Si substrate shows no such effects.

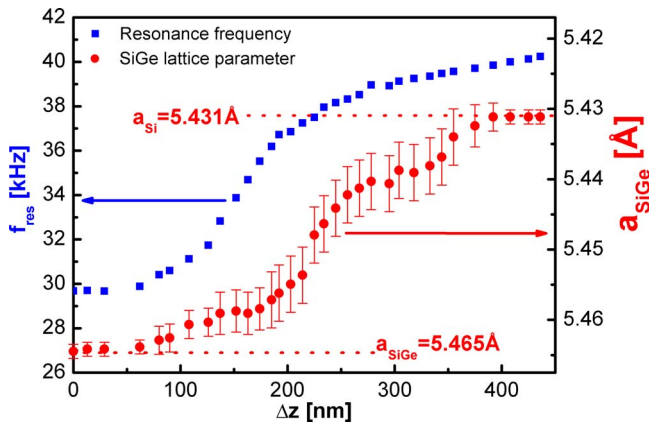


FIG. 3. (Color online) Variation of the SiGe island lattice parameter (red circles) as a function of the tuning fork displacement Δz . The tuning fork resonance frequency (blue squares), which varies considerably as the tip touches the island, follows the variation of the lattice parameter.

In general, due to the scattering geometry shown in Fig. 1(a), the 2D-RSMs represent a cut through reciprocal space at an angle corresponding to the (004) Bragg-condition of the SiGe island (in our case $\theta=28^\circ$). In the technique described so far, these RSMs do not contain the full information in reciprocal space. In the conventional method a three dimensional (3D)-RSM is obtained by rocking the sample in small steps, shifting thereby the detector-plane in reciprocal space perpendicular to the $\langle 001 \rangle$ direction. At each angle, a 2D diffraction image is recorded. From such a stack of tilted 2D-RSMs it is straightforward to reconstruct a 3D-RSM as shown in Fig. 2(a) (here, using simulated data).⁸ In the present case, however, with the AFM-tip in contact with the island, the vibrations induced by the stepper motor would instantly damage both the island and the tip. To avoid any movement of the diffractometer, we propose a different technique to obtain a 3D-RSM. By changing the incident x-ray photon energy, the detector plane will move in reciprocal space along the $\langle 001 \rangle$ direction. A stack of 2D-RSMs can then be recorded and used to obtain a 3D reconstruction of the intensity distribution. Such 3D-RSMs would be necessary to infer the complete change of island shape and strain distribution as it is pressed. For the current experiment, however, a 2D-RSM is sufficient to observe the variation of lattice parameter as a function of tip pressure (which is directly related to the applied pressure).

In order to correlate the lattice-parameter change with the applied pressure, a complete analysis of the mechanical setup is necessary. The tip-sample system is modeled as a series of coupled springs and the pressure is calculated taking into account the Hertzian contact model.¹⁰ Due to the interaction of the tip with the sample, its resonance frequency shifts to larger values. This variation is shown in Fig. 3, where the correlation between the SiGe island lattice parameter and the tip resonance frequency is directly visible. This frequency shift can be used to derive the applied force, and therefore the pressure. An initial estimation yielded a value of 200–300 μN for the applied force and 3–4 GPa for the corresponding pressure at the point where the SiGe lattice is completely compressed to the Si value [Fig. 2(d)]. Given the size of tip and island, as well as its composition, the estimated force is in good agreement with the one needed to induce the observed lattice parameter reduction assuming

the Young modulus of bulk $\text{Si}_{0.86}\text{Ge}_{0.14}$ ($E=126$ GPa), and that the tip applies an uniaxial pressure. A detailed description of the correlation between the resonance frequency of the tuning fork, the change of the lattice parameters and the applied force is out of the scope of this Letter and will be discussed elsewhere.¹¹ The SiGe island lattice parameter was obtained by determining the position of the center of mass of the island-induced x-ray diffraction signal [see ellipses in Figs. 2(c) and 2(d)] and translating it into an average island lattice parameter, corresponding to the distorted part of the single object. The variation of the SiGe island lattice parameter is continuous and quantitatively reproducible, showing that we are in the elastic regime of deformation and that no plastic deformation of the island occurred. This was also confirmed by scanning electron micrographs [Fig. 1(b)] taken before and after the experiment, revealing that the island remains intact.

In summary, we demonstrate the implementation of a powerful technique to investigate *in situ* the elastic properties of objects on the nanoscale. This combination of atomic force microscopy techniques [both imaging and manipulation of single (sub-)micron sized objects, particularly, pressure application] and x-ray diffraction paves the way to study a wide range of nanomaterials, such as nanotubes, nanowires, microelectro mechanical systems as well as pressure induced phase transitions. Additionally, the photoelectron current imaging provides a simple tool to align a microfocused beam to a selected nanostructure.⁷ The technique of using energy scans to obtain 3D reciprocal space maps is suggested to avoid the need of any movements of the diffractometer during the nanoindentation.

Financial support from the European Synchrotron Radiation Facility as well as the European Commission FP6 through Contract No. STRP 505634-1 X-Tip is greatly acknowledged. One of the authors (R.M.P.) acknowledges support from CNPq (Brazil). We thank M. Schmidbauer for supplying the sample.

- ¹J. Stangl, V. Holý, and G. Bauer, *Rev. Mod. Phys.* **76**, 725 (2004).
- ²G. Rubio-Bollinger, S. R. Bahn, N. Agrait, K. W. Jacobsen, and S. Vieira, *Phys. Rev. Lett.* **87**, 026101 (2001). Elastic properties of Ge nanostructures in the ultrasonic regime have already been studied by O. V. Kolosov, M. R. Castell, C. D. Marsh, G. A. D. Briggs, T. I. Kamins, and R. Stanley Williams, *Phys. Rev. Lett.* **81**, 1046 (1998).
- ³A. Saito, Y. Takagi, K. Takahashi, H. Hosokawa, K. Hanai, T. Tanaka, M. Akai-kasaya, Y. Tanaka, S. Shin, T. Ishikawa, Y. Kuwahara, and M. Aono, *Surf. Interface Anal.* **40**, 1033 (2008); V. Rose, J. W. Freeland, K. E. Gray, and S. K. Streiffer, *Appl. Phys. Lett.* **92**, 193510 (2008).
- ⁴See, e.g., T. U. Schüllli, J. Stangl, Z. Zhong, R. T. Lechner, M. Sztucki, T. H. Metzger, and G. Bauer, *Phys. Rev. Lett.* **90**, 066105 (2003).
- ⁵A. Snigirev, V. Kohn, I. Snigireva I. and B. Lengeler, *Nature (London)* **384**, 49 (1996).
- ⁶W. C. Oliver and G. M. Pharr, *J. Mater. Res.* **19**, 3 (2004).
- ⁷O. Dhez, M. Rodrigues, F. Comin, R. Felici, and J. Chevrier, *AIP Conf. Proc.* **879**, 1391 (2007).
- ⁸C. Mocuta, J. Stangl, K. Mundboth, T. H. Metzger, G. Bauer, I. A. Vartanyants, M. Schmidbauer, and T. Boeck, *Phys. Rev. B* **77**, 245425 (2008).
- ⁹M. Hanke, M. Dubsclaff, M. Schmidbauer, T. Boeck, S. Schöder, M. Burghammer, C. Riekel, J. Patommel, and C. G. Schroer, *Appl. Phys. Lett.* **92**, 193109 (2008).
- ¹⁰H. Hertz, *J. Reine Angew. Math.* **92**, 156 (1882).
- ¹¹M. S. Rodrigues, T. W. Cornelius, T. Scheler, C. Mocuta, A. Malachias, R. Magalhães-Paniago, O. Dhez, F. Comin, T. H. Metzger, and J. Chevrier (unpublished).
- ¹²See EPAPS Document No. E-APPLAB-94-030902 for a full series of diffraction patterns. For more information on EPAPS, see <http://www.aip.org/pubservs/epaps.html>.